Calculation of Supersonic Turbulent Reacting Coaxial Jets

Dean R. Eklund* and J. Philip Drummond†
NASA Langley Research Center, Hampton, Virginia
and
H. A. Hassan‡
North Carolina State University, Raleigh, North Carolina

The mixing and subsequent combustion within turbulent reacting shear layers is examined. To conduct this study, a computer program has been written to solve the axisymmetric Reynolds-averaged, Navier-Stokes equations. Turbulence is modeled using three algebraic turbulence models, and the chemical kinetics is modeled using a seven-species, seven-reaction, finite-rate chemistry model. Three separate flowfields are investigated. The effect of turbulent mixing upon the extent of combustion is demonstrated. No single turbulence model considered accurately predicted the degree of mixing for all three cases.

Introduction

RESEARCH is currently underway to develop advanced propulsion systems capable of sustaining hypersonic flight within the atmosphere. Due to the limitations of ground-test facilities and to the increase in computer capabilities, computational fluid dynamics (CFD) promises to play an integral role in the development of supersonic combustion ramjet (scramjet) technology.

The flowfield within a scramjet combustor is characterized by the interaction of several physical processes including turbulent fuel-air mixing and kinetically controlled combustion. The present study considers the problem of two coaxial streams mixing and burning within a free shear layer, which simulates the parallel injection of hydrogen fuel in a scramjet combustor. Though this flowfield does not possess the complexities arising from the geometry of a scramjet combustor, nevertheless, it does possess the fundamental physical interaction of a turbulent flow mixing and burning within a chemically reacting environment. This study of reacting shear layers is made in conjunction with a current experimental project at the NASA Langley Research Center to quantitatively examine the combustion of supersonic coaxial streams, and thereby, to provide a test of present numerical modeling capabilities.

Reacting flowfields are described by the Navier-Stokes equations augmented with appropriate species continuity equations that provide for the convection, diffusion, and production of each chemical species. Combustion within a supersonic stream is marked by short residence times. Hence, assuming complete or equilibrated combustion is often inaccurate. The finite rates of reaction are accounted for by introducing a multistep chemistry model to describe the reaction mechanism and then applying the law of mass action to determine the rates of production for each species.

Received Jan. 25, 1989; revision received Aug. 18, 1989.

*Research Associate, National Research Council. Member AIAA.
†Senior Research Scientist, Computational Methods Branch, Fluid Mechanics Division. Associate Fellow AIAA.
‡Professor, Mechanical and Aerospace Engineering. Associate Fellow AIAA.

Turbulent flows are considered in this work. The range of length scales and time scales present within a turbulent flowfield with finite-rate chemistry necessitates making simplifications in both the turbulent and the chemical kinetic formulations. In previous studies, a variety of turbulence models and chemical kinetics models for supersonic H_2-air reacting flows have been suggested. Evans et al.[1] employed a two-equation turbulence model and a one-equation (eddy breakup) chemical kinetics model based on the concept of unmixedness. The authors found that adjustments in the initial profiles of the turbulent kinetic energy and its dissipation were necessary between cases to achieve satisfactory agreement with experimental data. Adjustments to the constant in the eddy breakup model of over an order of magnitude were also found necessary to yield agreement with data.

Evans and Schexnayder[2] modified the computer program employed in Ref. 1 by replacing the eddy breakup model with alternately a 12-species, finite-rate chemistry model and Spiegler's seven-species[3] model. They found that the expanded reaction system was superior for the prediction of ignition. However, when ignition was known to be fast, the two kinetic systems gave nearly identical results.

Rogers and Chinitz[4] developed a global, five-species, two-step model for H_2-air combustion. Underprediction of the ignition delay period was observed using the global two-step model; however, when the ignition delay period was not long, good agreement was achieved between the global model and Spiegler's seven-species model.

Hitch et al.[5] made calculations for premixed flow in a one-dimensional adiabatic stream tube to isolate the kinetics effects. Calculations were made using the global two-step model developed by Rogers and Chinitz and also obtained using an eight-species model. The global model was shown to underpredict the ignition time and overpredict the reaction time.

Recently, Jachimowski[6] developed a 13-species, 33-reaction model for H_2-air combustion studies. Calculations were performed for quasi-one-dimensional combustor flows with Mach numbers of 8, 16, and 25. Mixing of fuel and oxidant was determined by a mixing routine, which set a prescribed schedule of mixing along the combustor. Results showed that the HO_2 chemistry had an important effect upon the calculated combustion efficiency of the Mach 8 nozzle (initial temperature equaled 670 K). However, the effect upon the chemical efficiency from the species HO_2 and H_2O_2 was only 6% for the Mach 16 nozzle (initial temperature equaled 1500 K) and was unappreciable for the Mach 25 nozzle (initial temperature equaled 2800 K).

Drummond et al.[7] and Drummond and Hussaini[8] conducted a detailed study of the structure of a spatially developing and reacting mixing layer and its associated flame. The chemical kinetics were modeled using a nine-species, 18-reaction model (Spark chemistry model) developed by Jachimowski.[9] Turbulence was not modeled in their study, but a multicomponent diffusion model was used to accurately model molecular diffusion.

In this study a computer program has been developed for predicting the combustion within supersonic coaxial jets. The H_2-air kinetics model of Drummond et al.[7] is employed. However, the reacting flows considered here have an initial temperature that enables rapid ignition. Hence, the species HO_2 and H_2O_2 plus the 11 reactions involving them are neglected. Turbulence is modeled using algebraic eddy viscosity turbulence models or mixing length models. Despite limitations inherent in these models, this study sought to investigate their performance over a variety of conditions. The numerical method adopted employs a central-difference, finite-volume approach and advances the solution forward in time using a Runge-Kutta scheme. The chemical source terms are treated in a point implicit manner to alleviate the stiffness in the equation set arising from the disparate time scales within the flowfield.[11,12]

In the first phase of this work, several turbulence models are evaluated for their ability to model the turbulent mixing of nonreacting supersonic coaxial H_2-air jets.[10] The aim of this phase is to eliminate those models that are unable to predict the experimental measurement from further consideration. The models selected were those of Eggers,[10] Cohen,[13] and Baldwin-Lomax.[14]

The second phase of this work was 1) to examine turbulent reacting flowfields using the kinetics model developed by Jachimowski[9] and 2) to assess the capability of the computer program developed to model these flowfields. Two experiments were chosen for comparison purposes. They are the reacting jet flow experiments conducted by Evans et al.[1] and by Jarrett et al.[15] at the NASA Langley Research Center.

Analysis

Equations of Motion

The equations describing viscous, chemically reacting flowfields are the Navier-Stokes equations augmented by appropriate species continuity equations. In an axisymmetric coordinate system, these partial differential equations can be written as

$$\frac{\partial}{\partial t}\boldsymbol{U}+\frac{\partial}{\partial x}\boldsymbol{F}(U)+\frac{1}{y}\frac{\partial}{\partial y}y\boldsymbol{G}(U)=\frac{\boldsymbol{H}(U)}{y} \tag{1}$$

where x and y are the streamwise and radial coordinates, respectively, and

$$\boldsymbol{U}=\begin{bmatrix}\rho\\ \rho u\\ \rho v\\ \rho E\\ \rho Y_i\end{bmatrix},\qquad \boldsymbol{F}=\begin{bmatrix}\rho u\\ \rho u^2+p-\tau_{xx}\\ \rho uv-\tau_{xy}\\ \rho uH-u\tau_{xx}-v\tau_{xy}+q_x\\ \rho uY_i+\rho\hat{V}_iY_i\end{bmatrix} \tag{2}$$

$$\boldsymbol{G}=\begin{bmatrix}\rho v\\ \rho uv-\tau_{xy}\\ \rho v^2+p-\tau_{yy}\\ \rho vH-v\tau_{yy}-u\tau_{xy}+q_y\\ \rho vY_i+\rho\check{V}_iY_i\end{bmatrix},\qquad \boldsymbol{H}=\begin{bmatrix}0\\ 0\\ p-\tau_{\theta\theta}\\ 0\\ y\dot{w}_i\end{bmatrix} \tag{3}$$

$$E=e+\frac{u^2+v^2}{2} \tag{4}$$

ρ is the density, u and v are the velocities in the x and y directions, p is the pressure, e is the internal energy, Y_i is the mass fraction of species i, and $\hat{V}_i$ and $\check{V}_i$ are the diffusion velocities of species i in the x and y directions. The enthalpy h and the stagnation enthalpy H are defined by

$$h\equiv e+\frac{p}{\rho},\qquad H=E+\frac{p}{\rho} \tag{5}$$

The viscous stresses are given by

$$\tau_{xx}=\lambda\left(\frac{\partial u}{\partial x}+\frac{\partial v}{\partial y}+\frac{v}{y}\right)+2\mu\frac{\partial u}{\partial x} \tag{6}$$

$$\tau_{yy}=\lambda\left(\frac{\partial u}{\partial x}+\frac{\partial v}{\partial y}+\frac{v}{y}\right)+2\mu\frac{\partial v}{\partial y} \tag{7}$$

$$\tau_{xy}=\mu\left(\frac{\partial u}{\partial y}+\frac{\partial v}{\partial x}\right) \tag{8}$$

$$\tau_{\theta\theta}=\lambda\left(\frac{\partial u}{\partial x}+\frac{\partial v}{\partial y}+\frac{v}{y}\right)+2\mu\frac{v}{y} \tag{9}$$

where μ and λ are the first and second coefficients of viscosity. The bulk viscosity is assumed negligible; hence,

$$\lambda+\frac{2}{3}\mu=0 \tag{10}$$

Neglecting the heat flux created by concentration gradients, the diffusion of energy contains two terms: the transport of heat according to Fourier's law of heat conduction and the transport of enthalpy due to mass diffusion.[16] Thus,

$$\boldsymbol{q}=-k\nabla T+\rho\sum_{i=1}^{ns}h_iY_i\vec{V}_i \tag{11}$$

where T, k, and ns are the temperature, coefficient of thermal conductivity, and the number of species in the mixture, respectively, and $\vec{V}_i$ is the diffusion velocity of species i.

The fluid of interest is a mixture of perfect gases. Hence, the equation of state takes the form

$$p=\rho RT,\qquad R=R_u\sum_{i=1}^{ns}\frac{Y_i}{W_i} \tag{12}$$

where W_i is the molecular weight of species i. The specific heat of each species is evaluated as a function of temperature from polynomial curve fits given in Ref. 17. The temperature is recovered from the internal energy by lagging values of the specific heat from the previous iteration.

Finally, $\dot{w}_i$ is the production rate of species i. The concentrations of the reacting species are evaluated by integrating a continuity equation, and the mass fraction of the inert species N_2 is determined from the conservation of mass statement

$$\sum_{i=1}^{ns}Y_i=1 \tag{13}$$

Transport Properties

The mixture coefficient of viscosity depends upon the temperature as well as the chemical composition of the gas. It is obtained from the following procedure. First, the species coefficients of viscosity are calculated from Sutherland's law

$$\frac{\mu_i}{\mu_{0i}}=\left(\frac{T}{T_{0i}}\right)^{1.5}\frac{T_{0i}+S_i}{T+S_i} \tag{14}$$

where μ_{0i}, T_{0i}, and S_i are the reference viscosity, reference temperature, and Sutherland coefficient of species i, respectively. The reference values for the individual species are

Table 1 Abridged Spark chemistry model

Reaction number	Reaction	A	b	T_a
1	$H_2 + O_2 \rightarrow OH + OH$	$0.170E+14$	0.0	24233
2	$H + O_2 \rightarrow OH + O$	$0.142E+15$	0.0	8254
3	$OH + H_2 \rightarrow H_2O + H$	$0.316E+08$	1.8	1525
4	$O + H_2 \rightarrow OH + H$	$0.207E+15$	0.0	6920
5	$OH + OH \rightarrow H_2O + O$	$0.550E+14$	0.0	3523
6	$H + OH \rightarrow H_2O + M$	$0.221E+23$	−2.0	0
7	$H + H \rightarrow H_2 + M$	$0.653E+18$	−1.0	0

Units of A are a multiple of $cm^3 \cdot mole^{-1} \cdot s^{-1}$.

tabulated in Refs. 18 and 19. The mixture coefficient of viscosity is then obtained by combining the species coefficients according to Wilke's formula.[20] Similarly, for the mixture coefficient of thermal conductivity, Sutherland's law is used to evaluate individual conductivity coefficients, which are then combined using Mason and Saxena's formula[20] to yield the mixture coefficient of thermal conductivity.

The diffusion of mass is determined by the diffusion velocities. Calculation of the diffusion velocities is simplified in this work by employing Fick's law of diffusion. As a consequence of Fick's law, the diffusion velocity of each species is directly related to the gradient of the concentration

$$\hat{V}_i = -D \frac{\partial}{\partial x} \ell n Y_i \tag{15}$$

where D is the binary coefficient. Although, Fick's law is not an accurate approximation for an H_2-air mixture, in the following turbulent calculations, molecular mixing (and any errors in its calculation) is typically one to two orders of magnitude smaller than mixing due to turbulence. The molecular binary diffusion coefficient in Eq. (15) is obtained by specifying a Le number, which is defined as

$$Le = \frac{k}{\rho C_p D} \tag{16}$$

Chemistry Model

The chemistry model used in this work is a modified version of the Spark model developed by Jachimowski[9] and employed by Drummond et al.[7] and Drummond and Hussaini.[8] It contains six reacting species: H_2, O_2, H_2O, OH, H, and O, plus an inert species N_2 that interacts through a seven-step reaction mechanism. The reactions together with the constants appearing in the Arrhenius expression for the forward rate coefficient k_{f_j}

$$k_{f_j} = A_j T^{b_j} \exp\left(\frac{-T_{a_j}}{T}\right) \tag{17}$$

are listed in Table 1.

The backward reaction rate coefficients k_{b_j} are obtained from the equilibrium constant K_j where

$$K_j = \frac{k_{f_j}}{k_{b_j}} \tag{18}$$

The equilibrium constants in the Spark chemistry model are obtained from the delta Gibbs function for each reaction ΔG_j^0 according to the relation[21]

$$K_j = \left(\frac{1}{R_u' T}\right)^{\Delta n_j} \exp\left(\frac{-\Delta G_j^0}{R_u T}\right) \tag{19}$$

where Δn_j is the change in the number of moles going from the reactants to products, and R_u' is the universal gas constant in l-atm/kg-mole-K. (The Gibbs function is evaluated as in Ref. 22.) The chemical production terms are evaluated from the reaction rates and the chemical composition of the gas by using the law of mass action as given in Ref. 16.

Turbulence Models

Equations for the mean motions of the turbulent flow are solved in this work. Following Favre,[23] the dependent variables are decomposed into mass weighted averages

$$f = \tilde{f} + f'', \qquad \tilde{f} \equiv \frac{\overline{\rho f}}{\bar{\rho}} \tag{20}$$

where the overbar represents averaging with respect to time. The decomposed variables are substituted into the instantaneous equations, which are then averaged over time to yield[24]

$$\frac{\partial}{\partial t} \boldsymbol{U} + \frac{\partial}{\partial x} [\boldsymbol{F}(U) + \boldsymbol{F}_t(U)] + \frac{1}{y} \frac{\partial}{\partial y} y[\boldsymbol{G}(U) + \boldsymbol{G}_t(U)] = \frac{\boldsymbol{H}(U)}{y} \tag{21}$$

The vectors $\boldsymbol{U}$, $\boldsymbol{F}$, $\boldsymbol{G}$, and $\boldsymbol{H}$ above are equivalent to the corresponding vectors in Eqs. (2) and (3) except that the dependent variables represent mean rather than instantaneous values. The vectors $\boldsymbol{F}_t$ and $\boldsymbol{G}_t$ contain the additional unknowns introduced by averaging that represent the effect of the turbulent fluctuations upon the mean flow. $\boldsymbol{F}_t$ is given by

$$\boldsymbol{F}_t = \begin{bmatrix} 0 \\ \overline{\rho u'' u''} \\ \overline{\rho u'' v''} \\ \tilde{u}\overline{\rho u'' u''} + \tilde{v}\overline{\rho u'' v''} + \overline{\rho u'' h''} - \overline{\rho D \sum_{i=1}^{ns} h_i \frac{\partial Y_i''}{\partial x}} + t_1 \\ \overline{\rho u'' Y_i''} + t_2 \end{bmatrix} \tag{22}$$

where

$$t_1 = \overline{u''\left(\tau_{xx} + \frac{\rho u'' u''}{2}\right)} + \overline{v''\left(\tau_{xy} + \frac{\rho u'' v''}{2}\right)} \tag{23}$$

and

$$t_2 = \overline{-\rho D \frac{\partial Y_i''}{\partial x}} \tag{24}$$

($\boldsymbol{G}_t$ is given in Ref. 26.) In this work, the terms given in Eqs. (23) and (24) are neglected. The remaining terms are modeled using an eddy-viscosity formulation.

Eddy-viscosity models relate the turbulent stresses and fluxes directly to the gradients of the mean flow through an

eddy-viscosity coefficient μ_t. For example,

$$\begin{bmatrix} \overline{\rho u'' v''} \\ \overline{\rho u'' h''} \\ \overline{\rho u'' Y''} \end{bmatrix} = \begin{bmatrix} -\mu_t\left(\dfrac{\partial \tilde{u}}{\partial y} + \dfrac{\partial \tilde{v}}{\partial x}\right) \\ -k_t\left(\dfrac{\partial \tilde{T}}{\partial x}\right) \\ -\bar{\rho} D_t\left(\dfrac{\partial \tilde{Y}}{\partial x}\right) \end{bmatrix} \tag{25}$$

where

$$k_t = C_p \frac{\mu_t}{Pr_t}, \qquad D_t = \frac{k_t}{\bar{\rho} C_p Le_t} \tag{26}$$

and Pr_t and Le_t are the turbulent Prandtl and Lewis numbers, respectively.

Note, the equations associated with the chemistry models are assumed to also apply to the turbulent mean values. Hence, the effect of fluctuations in the concentration values on the chemical production terms, the effect of temperature fluctuations on the reaction rate coefficients, as well as the effect of the concentration and temperature fluctuations on the equation of state are ignored.

From the above, the Reynolds-averaged equations become equivalent to the instantaneous Navier-Stokes equations except for modifications to the transport coefficients. The effective viscosity coefficient, for example, takes the form

$$\mu = \mu_l + \mu_t \tag{27}$$

where the subscripts l and t refer to the laminar and the turbulent components, respectively.

Models for the evaluation of the eddy viscosity μ_t for jet flow take the general form first proposed for incompressible flow by Prandtl[25]

$$\mu_t = c\rho V L \tag{28}$$

where c is an empirically determined constant, V is a characteristic velocity scale, and L is the width of the mixing layer. Individual models differ primarily in how the characteristic scales are evaluated.

Eggers Turbulence Model

The Eggers algebraic mixing length model[10] is defined as

$$\mu_t = c_e \rho u_0 z \tag{29}$$

where c_e is a constant, u_0 is the streamwise velocity on the jet centerline, and z is the width of the mixing layer. This width is defined as the radial distance between the points in the profile where the local velocities u_1 and u_2 are given by the following equations:

$$u_1 = u_a + 0.95(u_0 - u_a) \tag{30}$$

$$u_2 = u_a + 0.5(u_0 - u_a) \tag{31}$$

where u_a is the velocity in the external flow of the outer jet, and u_0 is the centerline velocity.

Cohen Turbulence Model

Cohen modified Prandtl's model to formally account for density variations across the mixing layer and to account for the turbulence initially present in the jets.[13] His model is defined by the following equations:

$$\mu_t = c_c \rho u_0 (1-m)\left(f\frac{1+n}{2}\right)^{0.8} z, \qquad m \le m_1 \tag{32}$$

$$\mu_t = c_c \rho u_0 (1-m_1)\left(\frac{1+n_1}{2}\right)^{0.8}\left(\frac{1+n_1}{1+n}\right)\left(\frac{1+mn}{1+m_1 n_1}\right) z \qquad m \ge m_1 \tag{33}$$

where z is the width of the mixing layer, m is the velocity ratio u_a/u_0, n is the density ratio ρ_a/ρ_0, f is an additional empirical constant, and m_1 is a velocity ratio fixed by the turbulence level which, as in Ref. 10, was set equal to 0.4. The value of n_1 is calculated at the axial location where $m = m_1$. Two modifications were made to the Cohen model. First, following Eggers, a single leading coefficient c_c was used through both the potential core and the far flowfield, and second, the definition of the mixing length used in Eggers model was also used in the Cohen model. For flowfields where the velocity ratio m is everywhere greater than m_1, which is true for all of the cases considered in this work, the Cohen turbulence model reduces to Eq. (33).

Baldwin-Lomax Turbulence Model

The Baldwin-Lomax model[14] for the outer region of turbulent-wall boundary layers was designed to be used in wakes as well. It is defined as

$$\mu_t = c_b \rho F_{\text{Wake}} F_{\text{Kleb}}(y) \tag{34}$$

where F_{Wake} is defined as the smaller of the following two expressions

$$F_{\text{Wake}} = y_{\max} F_{\max} \tag{35}$$

$$F_{\text{Wake}} = C_{wk} y_{\max} u_{\text{diff}}^2 / F_{\max} \tag{36}$$

$F_{\text{Kleb}}(y)$ is the Klebanoff intermittency factor, u_{diff} is the difference between the maximum and minimum total velocities in the profile, and C_{wk} is an additional empirical constant equal to 0.25. The function F is defined as

$$F(y) = y|\omega| \tag{37}$$

where ω is the vorticity. The quantity $F_{\max}$ is the maximum value of $F(y)$ that occurs in a profile and $y_{\max}$ is the value of y at which it occurs. Hence, the distribution of vorticity is used to determine the length scale.

Solution Technique

The stiffness associated with the chemical production terms is counteracted in this work by treating the source term implicitly, and then linearizing to form a preconditioning matrix S. That is, writing the source term implicitly and linearizing

$$\frac{\boldsymbol{H}^{n+1}}{y} = \frac{\boldsymbol{H}^n}{y} + \frac{1}{y}\frac{\partial \boldsymbol{H}^n}{\partial \boldsymbol{U}}\frac{\partial \boldsymbol{U}^n}{\partial t}\Delta t + \mathcal{O}(\Delta t^2) \tag{38}$$

Substituting Eq. (38) into Eq. (1) then yields

$$S^n \frac{\partial}{\partial t}\boldsymbol{U}^n + \frac{\partial}{\partial x}\boldsymbol{F}^n + \frac{1}{y}\frac{\partial}{\partial y} y\boldsymbol{G}^n = \frac{\boldsymbol{H}^n}{y} \tag{39}$$

where

$$S^n = I - \frac{1}{y}\frac{\partial \boldsymbol{H}^n}{\partial \boldsymbol{U}}\Delta t \tag{40}$$

The preconditioning matrix S acts to rescale the time step so that each equation is advanced at its own characteristic time scale.[12] Evaluation of the Jacobian matrix $\partial \boldsymbol{H}/\partial \boldsymbol{U}$ is simplified by neglecting the temperature dependence of the source term. This procedure has been found to be an efficient treatment of the preconditioning matrix.[27]

The finite volume or integral method for solving Eq. (39) is performed by first integrating around an arbitrary cell

$$\int\int\int\left[S^n\frac{\partial}{\partial t}U^n+\frac{\partial}{\partial x}F^n+\frac{1}{y}\frac{\partial}{\partial y}yG^n=\frac{H^n}{y}\right]y\,dy\,dx\,d\theta \quad (41)$$

Applying Leibniz's rule to the time derivative and taking the value at the cell center to be the average value for U and H yields

$$S^n\frac{\partial}{\partial t}U^n+\frac{1}{V}\int\int\left[\frac{\partial}{\partial x}(yF^n)+\frac{\partial}{\partial y}(yG^n)\right]dy\,dx=\frac{A}{V}H^n \quad (42)$$

where V is the volume of the cell divided by 2π, and A is the area of the cell in a constant θ plane. Applying the divergence theorem, integrating in the clockwise direction, and discretizing using the midpoint integration rule yields

$$S^n\frac{\partial}{\partial t}U^n=-\frac{1}{A}\sum_{k=1}^{4}\left(-\frac{y}{y_c}F^n\Delta y+\frac{y}{y_c}G^n\Delta x\right)_k+\frac{H^n}{y_c} \quad (43)$$

where

$$y_c\equiv\frac{V}{A} \quad (44)$$

The inviscid portion of the flux is calculated from the dependent variables at the midpoint of the cell sides. The values at the cell sides are determined by averaging the values at the two adjacent cell centers. On rectangular grids, this finite volume treatment is equivalent to second-order central differencing. Calculating the flux of the viscous or diffusive terms requires evaluating derivatives at the cell sides. This is achieved by again employing the divergence theorem and the midpoint integration rule.[29] The calculation is simplified by making the thin layer approximation, which states that the viscous gradients in the streamwise direction are negligible compared to the viscous gradients in the normal direction.

Once the flux balance is evaluated, the residual is obtained by matrix inversion using a Householder routine modified for the Cray computers by Lambiotte.[30] The result is a system of differential equations at each grid point of the form

$$\frac{\mathrm{d}}{\mathrm{d}t}U=R(U,t) \quad (45)$$

The solution is advanced using a modified, four-stage, Runge-Kutta scheme with the maximum allowable local time step. The local time step is calculated by combining the convective time scale, Δt_c, and the diffusive time scale, Δt_d, according to[31]

$$\frac{1}{\Delta t}=\frac{1}{\Delta t_c}+\frac{1}{\Delta t_d} \quad (46)$$

The individual components of the convective and the diffusive time steps are based on the stability limit for solving the advection equation and the heat equation, respectively, using central differences.

Results

Eggers Nonreacting Mixing Layer

The theory and the numerical method described in the previous sections were applied to three H_2-air coaxial jet-flow experiments. The first experiment considered was conducted by Eggers[10] and was used in this work to evaluate the eddy-viscosity turbulence models detailed earlier. The schematic of the coaxial jet flowfields examined in this work is shown in Fig. 1. The Eggers flowfield was a cold flow so that a mixing layer but not a flame develops. The temperature and the other exit conditions for the nozzle are given in Table 2.

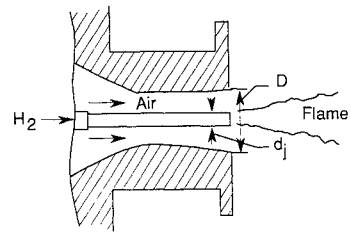

Fig. 1 Schematic for the coaxial jet flowfields considered in this study.

Table 2 Exit conditions for the Eggers experiment

Exit conditions	Hydrogen jet	Outer jet
Mach number	0.9	2.5
Temperature, K	260	140
Velocity, m/s	1107	609
Pressure, MPa	0.101	0.101
Mass fraction		
Y_{H_2}	1	0
Y_{O_2}	0	0.233
Y_{N_2}	0	0.767
Y_{H_2O}	0	0

Fuel injector inner diameter = 0.0116 m.
Lip thickness = 0.00055 m.
Nozzle diameter = 0.152 m.

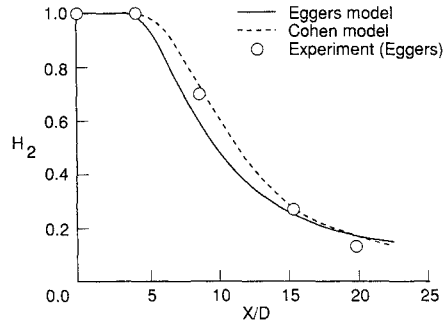

Fig. 2 Centerline distribution of the hydrogen mass fraction for the Eggers flowfield calculated using the Eggers and Cohen turbulence models.

The computational grid used for the following calculations is 61 × 61 with grid stretching in the transverse direction at the interface between the coaxial jets. The grid extended 22.5 fuel-injector inner diameters ($D = 0.0116$ m) in the flow direction and 3 diam in the transverse direction.

The variables along the inflow plane, which corresponds to the jet exit, were determined from values for T_0, u, v, p, and Y_i. All values were specified except the pressure. The pressure was specified along the boundary of the supersonic outer jet and extrapolated from the interior of the computational domain along the boundary of the subsonic inner jet. Also, the velocity was specified from a spline fit of experimental values. The treatment of the upper, outer, and centerline boundaries was identical for each of the three cases considered. Values along the upper boundary and the outer boundary were obtained by extrapolation assuming a zero gradient. Values along the centerline boundary were also obtained by extrapolation assuming a zero gradient, except the transverse velocity, which was set equal to zero. Values at each axial station

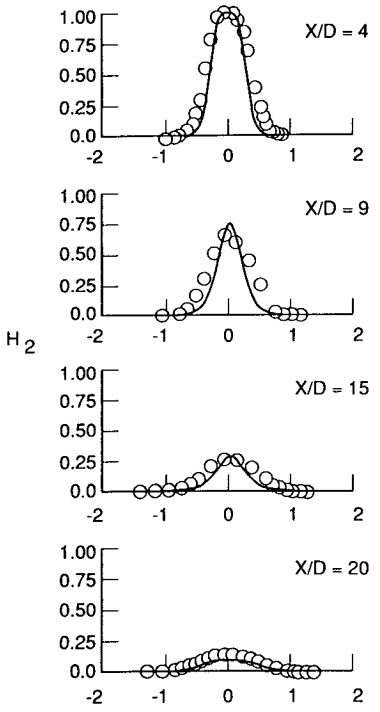

Fig. 3 Hydrogen mass fraction profiles at four axial locations for the Eggers flowfield calculated using the Cohen turbulence model.

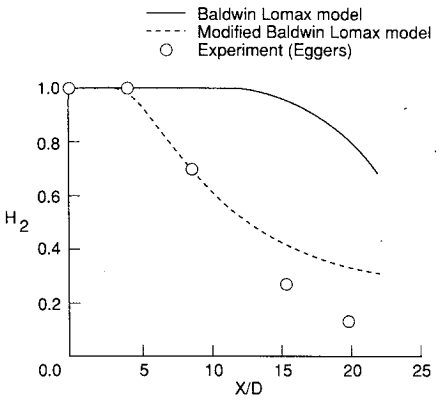

Fig. 4 Centerline distribution of the hydrogen mass fraction for the Eggers flowfield calculated using the Baldwin Lomax and a modified Baldwin-Lomax turbulence model.

of the computational domain were initialized equal to the values along the inflow boundary.

The integrations were advanced 2500 iterations, for this case, after which the $L2$ norm of the residual taken over the entire solution domain dropped between five and six orders of magnitude.

Calculations were first made using the turbulence models developed by Eggers and Cohen. As in Eggers' study,[10] the leading constant in the Eggers model was taken to be 0.0164, and the turbulent Prandtl and Lewis numbers were set equal to 0.9 and 1, respectively. In the Cohen model, the leading constant was taken to be 0.0024, and the turbulent Prandtl and Lewis numbers were both set equal to one.

Comparison of the H_2 mass fraction distribution along the centerline using the Eggers and Cohen model is shown in Fig. 2. Both models provide a good prediction of the extent of mixing within the shear layer; although, the Cohen model provides slightly better agreement with experimental data. Figure 3 shows the computed hydrogen profiles using the Cohen model at four axial locations. A calculation was repeated using a refined 99 × 99 grid. The solutions on the two grids were very similar indicating that the 61 × 61 grid provided sufficient resolution for this case.

Calculations were then made using the Baldwin-Lomax model with coefficients taken from Ref. 14. The resulting mass fraction predictions along the centerline are shown in Fig. 4. The vorticity is very large within the initial profile. Hence, the characteristic length scale, obtained by dividing the velocity difference by the maximum vorticity, is small. Consequently, the mixing is greatly underpredicted in the early portion of the solution. This problem was addressed by artificially limiting the calculated value of the vorticity. Results from this modified Baldwin-Lomax model are also shown in Fig. 4. The plot of the centerline distribution of the hydrogen mass fraction indicates that even when sufficient mixing is predicted initially, the extent of the mixing is still underpredicted at the last two experimental locations. Consequently, the Baldwin-Lomax model was not used for the two reacting coaxial jet-flow calculations.

Table 3 Exit conditions for the Beach experiment

Exit conditions	Hydrogen jet	Outer jet
Mach number	2	1.9
Temperature, K	251	1495
Velocity, m/s	2418	1510
Pressure, MPa	0.100	0.100
Mass fraction		
Y_{H_2}	1	0
Y_{O_2}	0	0.241
Y_{N_2}	0	0.478
Y_{H_2O}	0	0.281

Fuel injector inner diameter = 0.006525 m.
Lip thickness = 0.0015 m.
Nozzle diameter = 0.0653 m.

Beach Reacting Coaxial Jet Case

The first reacting, coaxial, jet-flow case considered was the experiment conducted by Evans et al.[1] The conditions at the exit of the burner lip are given in Table 3. The computational grid used for this case is 61 × 71. A finite thickness lip was assumed in these calculations, and grid stretching was employed at the lip edges. The grid extended 30 fuel-injector outer diam (D = 0.009525 m) in the flow direction and 2 diam in the transverse direction.

Uniform conditions were used at the inflow boundary for both the inner and outer jets. Along the jet lip, no-slip and noncatalytic wall conditions were assumed. Also, the temperature was assumed to vary linearly along the lip between the inner and outer jet values and the pressure along the lip was obtained by extrapolation.

Calculations were performed using the abridged Spark chemistry model and both the Eggers and the Cohen turbulence models. The coefficients for the two models were left unchanged from the values used in the previous case. The integrations were advanced 6000 iterations after which the residual dropped approximately five orders of magnitude. A calculation using the Cohen model was also made on a refined 151 × 101 grid. Differences between the solutions on the two grids were small.

Figure 5 compares with H_2 mass-fraction distribution along the centerline using the two turbulence models. The mass fraction of H_2 calculated along the centerline using the Eggers turbulence model is smaller than the experimental values. The calculated mass fraction using the Cohen turbulence model remains 1 along the centerline until x/d exceeds 25. As evidenced by the centerline distribution of H_2, the Eggers

model overpredicts the extent of mixing, and the Cohen model severely underpredicts the extent of mixing.

Figure 6 compares the combustion efficiency for the two solutions. The combustion efficiency is defined as $1-(m_{H2}/m_{HT})/(m_{H2}/m_{HT})_0$ where m_{H2} is the mass flow rate of diatomic hydrogen, m_{HT} is the mass flow rate of hydrogen in all forms and the subscript 0 designates the inflow plane. Hence, the value of the combustor efficiency scales from 0 to 1. Figure 5 indicates a greater degree of combustion for the solution

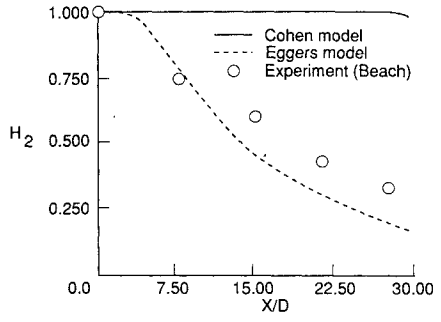

Fig. 5 Centerline distribution of the hydrogen mass fraction for the Beach case.

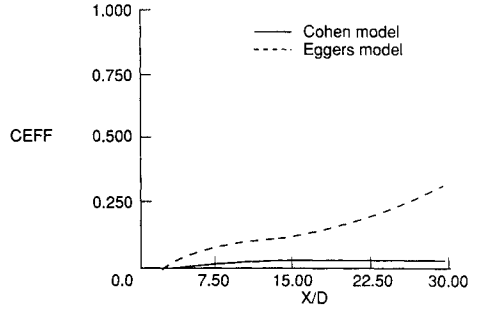

Fig. 6 Axial variation of the combustion efficiency for the Beach case.

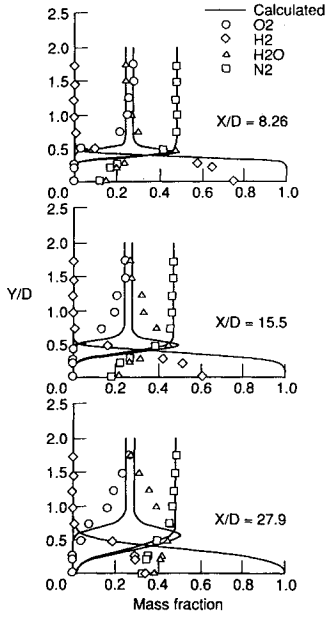

Fig. 7 Mass fraction profiles at three axial locations for the Beach case calculated using the Cohen turbulence model.

using the Eggers model. As expected, increased mixing results in increased combustion.

Figures 7 and 8 show the calculated profiles of four species vs experimental data taken at three axial locations using the Eggers and Cohen turbulence models, respectively. The three calculated profiles with positive values at y/D are, from left to right, the mass fraction of O_2, H_2O and N_2. The calculated profile with a value of zero at $y/D=2$ is the mass fraction of H_2. In Fig. 7, at the axial location $x/D=8.26$, the profile of the H_2O mass fraction reveals a knee. This knee indicates the presence of combustion in the solution using the Cohen turbulence model. The knee in the calculated H_2O mass fraction obtained using the Eggers model, shown in Fig. 8, has approximately the same peak but is broader than the knee at the corresponding axial location in Fig. 7. At succeeding axial locations the knee in the H_2O mass fraction grows and spreads faster in the solution using the Eggers turbulence model (see Fig. 8) as compared to the solution using the Cohen turbulence model (see Fig. 7). The mass fractions of H_2 and N_2 are also seen to spread faster in the Eggers solution.

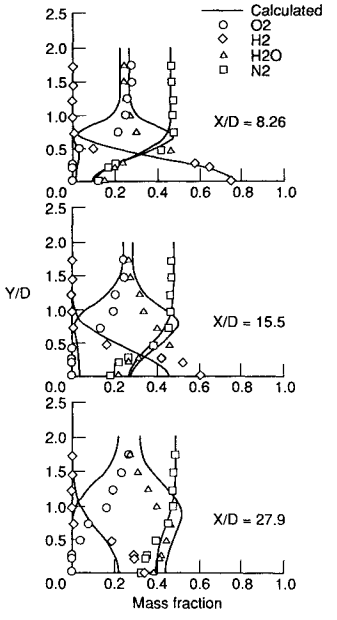

Fig. 8 Mass fraction profiles at three axial locations for the Beach case calculated using the Eggers turbulence model.

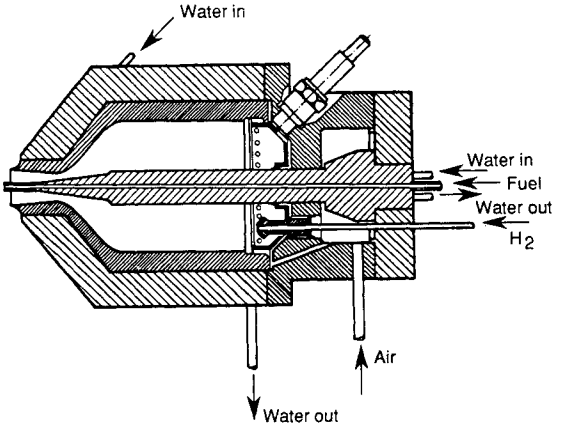

Fig. 9 Schematic of the apparatus for the Jarrett experiment.

Table 4 Exit conditions for the Jarrett experiment

Exit conditions	Hydrogen jet	Outer jet	Ambient jet
Mach number	1	2.02	0
Temperature, K	545	1250	273
Velocity, m/s	1772	1441	0
Pressure, MPa	0.112	0.096	0.101
Mass fraction			
Y_{H_2}	1	0	0
Y_{O_2}	0	0.254	0.233
Y_{N_2}	0	0.572	0.767
Y_{H_2O}	0	0.174	0

Fuel injector inner diameter = 0.00132 m.
Lip thickness = 0.00145 m.
Nozzle diameter = 0.01778 m.

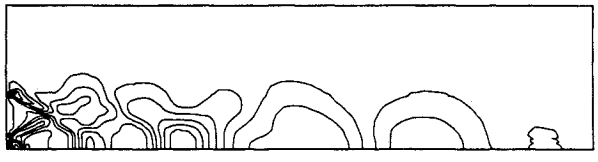

Fig. 10 Calculated pressure contours for the Jarrett case.

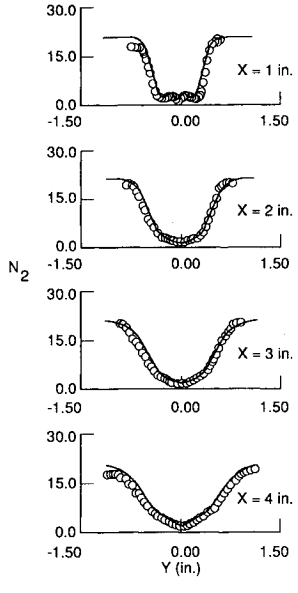

Fig. 11 Nitrogen number density ($\times 10^{-18}$) profiles at four axial locations for the Jarrett flowfield.

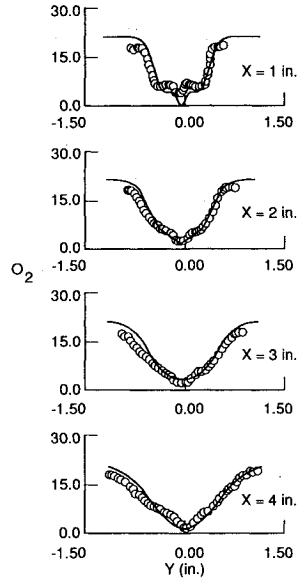

Fig. 12 Oxygen number density ($\times 10^{-18}$) profiles at four axial locations for the Jarrett flowfield.

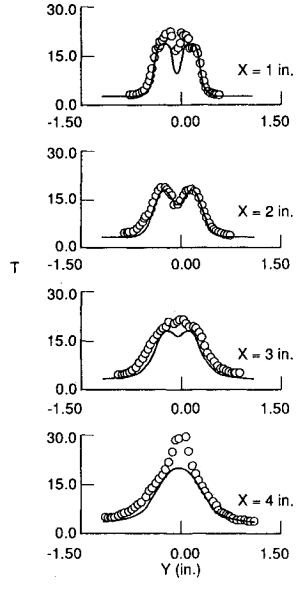

Fig. 13 Temperature (K) profiles at four axial locations for the Jarrett flowfield.

Jarrett Reacting Coaxial Jet Case

The second reacting jet-flow case considered was the experiment recently conducted by Jarrett et al.[15] at the NASA Langley Research Center. The burner with the flow from right to left is depicted in Fig. 9. At its exist, the nozzle has an angle of 4.3 deg with respect to the centerline. The walls of the nozzle of the burner were conical. The geometry of the tip of the fuel injector was a cone connected to a cylinder as shown in Fig. 9. A shock wave emanates from this juncture, which lends uncertainty to the jet exit conditions which are given in Table 4.

The computational grid used for this case is 61 × 61. The computational domain extended beyond the nozzle lip into the ambient air 3.65 in. The thickness of the burner lip, but not the nozzle lip, was accounted for in the computational domain. Grid stretching in the transverse direction was employed at the interface of the inner jet and the jet lip, at the interface of the jet lip and the outer jet, and at the interface of the outer jet and the ambient air. The grid extended 4 in. or 86 inner diam in both the flow direction and the transverse direction.

The inflow boundary was treated like the inflow boundary in the Beach case except for the region in the ambient air. In this region the streamwise velocity was extrapolated from the interior, and the other variables were specified.

Calculations were performed using a modified Eggers turbulence model. Because the computational domain extended into the ambient air, the definition of the mixing length given by Eqs. (30) and (31) was adjusted. Rather than base the mixing length on the profile of velocity, the mixing length was determined from the profile of diatomic hydrogen. That is, Eqs. (30) and (31) were retained, but the velocity was re-

placed with the mass fraction of H_2. The leading coefficient was also increased to 0.032.

Figure 10 shows the pressure contours for the calculated solution. The flow is from left to right. The interaction of the expanding outer jet with the ambient air produces a shock wave emanating from the corner of the nozzle. This shock wave hits the centerline producing a series of expansion and compression regions. Figures 11 and 12 show the profiles of the number density of N_2 and O_2, respectively, vs experimental data (circles) at four axial locations. (Density values were not experimentally obtained; therefore the experimental mass fractions could not be determined.) The extent of the mixing is reasonably well predicted using the modified Eggers turbulence model. Figure 13 shows the temperature profiles vs experimental data at the same four axial locations. The temperature peak is underpredicted at the fourth axial station in this solution. It is suspected that the strength of the shock structure near the rear of the computational domain is not accurately predicted in the solution.

Concluding Remarks

A computational program has been developed for modeling turbulent reacting flowfields. Three turbulent coaxial jet flowfields were calculated. Several algebraic, eddy-viscosity turbulent models were investigated. The Baldwin-Lomax turbulence model was found to be ill suited for predicting the turbulent mixing within free shear layers (especially in the near-jet region); however, no single turbulence model accurately predicted the extent of mixing for all three cases. The chemical reaction mechanism was described using a seven-reaction model involving seven chemical species. The extent of combustion was found to depend upon the extent of turbulent mixing predicted. The chemistry model yielded qualitative agreement with experimental results when the mixing was well represented.

Acknowledgments

This work is supported in part by the following grants: NASA Grant NAG-1-244, the Hypersonics Aerodynamics Program Grant NAGW-1022 funded jointly by NASA, the Air Force Office of Scientific Research and Office of Naval Research; and the Mars Mission Center funded by NASA Grant NAGW-1331. D. Eklund would like to acknowledge helpful discussions with Tawitt Chitsomboon, J. Lambiotte and Mark Carpenter.

References

[1]Evans, J. S., Schexnayder, C. J., Jr., and Beach, H. L., Jr., "Application of a Two-Dimensional Parabolic Computer Program to Prediction of Turbulent Reacting Flows," NASA TP-1169, 1978.

[2]Evans, J. S., and Schexnayder, C. J., Jr., "Influence of Chemical Kinetics and Unmixedness on Burning in Supersonic Hydrogen Flames," *AIAA Journal*, Vol. 18, Feb. 1980.

[3]Spiegler, E., Wolfshtein, M., and Manheimer-Timmat, Y., "A Model of Unmixedness for Turbulent Reacting Flows," *Acta Astronautica*, Vol. 3, March–April 1976, pp. 265–280.

[4]Rogers, R. C., and Chinitz, W., "Using a Global Hydrogen-Air Combustion Model in Turbulent Reacting Flow Calculations," *AIAA Journal*, Vol. 21, April 1983, pp. 586–593.

[5]Hitch, B. D., Laster, W. R., Sewser, D. W., and Sojka, P. E., "On the Selection of H_2/Air Kinetic Mechanisms for Use in Supersonic Combustor Modeling," Spring 1986 Technical Meeting of the Central States Section of the Combustion Institute, Cleveland, May 1986.

[6]Jachimowski, C. J., "An Analytical Study of the Hydrogen-Air Mechanism with Application to Scramjet Combustion," NASA TP-2791, 1988.

[7]Drummond, J. P., Rogers, R. C., and Hussaini, M. Y., "A Detailed Numerical Model of a Supersonic Reacting Mixing Layer," AIAA Paper 86-1427, June 1986.

[8]Drummond, J. P., and Hussaini, M. Y., "Numerical Simulation of a Supersonic Reacting Mixing Layer," AIAA Paper 87-1325, June 1987.

[9]Jachimowski, C. J., "An Analytical Study of the Hydrogen-Air Reaction Mechanism with Application to Scramjet Combustion," NASA TP 2791, 1988.

[10]Eggers, J. M., "Turbulent Mixing of Coaxial Compressible Hydrogen-Air Jets," NASA TN D-6487, 1971.

[11]Widhopf, G. F., and Victoria, K. J., "On the Solution of the Unsteady Navier-Stokes Equations Including Multicomponent Finite Rate Chemistry," *Computers and Fluids*, Vol. 1, June 1973, pp. 159–184.

[12]Bussing, T. R. A., and Murman, E. M., "A Finite Volume Method for the Calculation of Compressible Chemically Reacting Flows," AIAA Paper 85-0331, Jan. 1985.

[13]Cohen, L. S., and Guile, R. N., "Measurements in Freejet Mixing/Combustion Flows," *AIAA Journal*, Vol. 8, June 1970, pp. 1053–1061.

[14]Baldwin, B. S., and Lomax, H., "Thin Layer Approximation and Algebraic Model for Separated Turbulent Flows," AIAA Paper 78-257, Jan. 1978.

[15]Jarrett, O., Jr., Cutler, A. D., Antcliff, R. R., Chitsomboon, T., Dawley, C. L., and Wang, J. A., "Measurements of Temperature, Density, and Velocity in Supersonic Reacting Flow for CFD Code Validation," 25th JANNAF Combustion Meeting, Oct. 1988.

[16]Williams, F. A., *Combustion Theory*, Benjamin/Cummings Publ. 1985.

[17]McBride, B. J., Heimel, S., Ehlers, J., and Gordon, S., "Thermodynamic Properties to 6000 K for 210 Substances Involving the First 18 Elements," NASA SP-3001, 1963.

[18]White, F. M., *Viscous Fluid Flow*, McGraw-Hill, New York, 1974, pp. 27–36.

[19]Suehla, R. A., "Estimated Viscosities and Thermal Conductivities of Gases at High Temperatures," NASA TR-R-132, 1962.

[20]Dorrance, W. H., *Viscous Hypersonic Flow*, McGraw-Hill, New York, 1962, pp. 275–279.

[21]Kanury, A. M., *Introduction To Combustion Phenomena*, Gordon and Breach, New York, 1982, pp. 363–369.

[22]Wark, K., *Thermodynamics*, McGraw-Hill, New York, 1977, pp. 619–621.

[23]Favre, A., "Equations des Gaz Turbulents Compressibles," *Journal de Mecanique*, Vol. 4, No. 3, Sept. 1965, pp. 361–390.

[24]Rubesin, M. W., and Rose, W. C., "The Turbulent Mean-Flow, Reynolds-Stress and Heat-Flux Equations in Mass-Averaged Dependent Variables," NASA TM-X-62,248, 1973.

[25]Prandtl, L., "Bemerkungen zur Theorie der freien Turbulenz," *ZAMM*, Vol. 22, Oct. 1942, pp. 241–243.

[26]Eklund, D. R., "Numerically Modeling of Supersonic Turbulent Reacting Free Shear Layers," Ph.D. Dissertation, North Carolina State Univ., Raleigh, NC, May 1989.

[27]Eklund, D. R., Drummond, J. P., and Hassan, H. A., "The Efficient Calculation of Chemically Reacting Flow," AIAA Paper 86-0563, Jan. 1986.

[28]Jameson, A., Schmidt, W., and Turkel, E., "Numerical Solutions of the Euler Equations by Finite Volume Methods Using Runge-Kutta, Time-Stepping Schemes," AIAA Paper 81-1259, June 1981.

[29]Swanson, R. C., and Turkel, E., "A Multistage Time-Stepping Scheme for the Navier-Stokes Equations," AIAA Paper 85-0035, Jan. 1985.

[30]Lambiotte, J. J., Jr., unpublished work, Aug. 1988.

[31]Arnone, A., and Swanson, R. C., "A Navier-Stokes Solver for Cascade Flows," NASA CR 181682, July 1988.